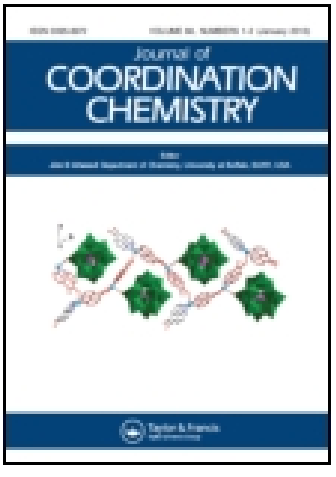

Journal of Coordination Chemistry
Publication details, including instructions for authors and subscription information:
http://www.tandfonline.com/loi/gcoo20

Syntheses, crystal structures, and antibacterial activities of helical M(II) phenyl substituted pyrazole carboxylate complexes

Hong Liu[a], Gao-Shan Yang[a], Chong-Bo Liu[a], Yi Lin[a], Yi Yang[a] & Yun-Nan Gong[a]

[a] School of Environment and Chemical Engineering, Nanchang Hangkong University, Nanchang, PR China

Accepted author version posted online: 24 Feb 2014.Published online: 02 Apr 2014.

To cite this article: Hong Liu, Gao-Shan Yang, Chong-Bo Liu, Yi Lin, Yi Yang & Yun-Nan Gong (2014) Syntheses, crystal structures, and antibacterial activities of helical M(II) phenyl substituted pyrazole carboxylate complexes, Journal of Coordination Chemistry, 67:4, 572-587, DOI: 10.1080/00958972.2014.896993

To link to this article: http://dx.doi.org/10.1080/00958972.2014.896993

Journal of Coordination Chemistry, 2014
Vol. 67, No. 4, 572–587, http://dx.doi.org/10.1080/00958972.2014.896993

Syntheses, crystal structures, and antibacterial activities of helical M(II) phenyl substituted pyrazole carboxylate complexes

HONG LIU, GAO-SHAN YANG, CHONG-BO LIU*, YI LIN, YI YANG and YUN-NAN GONG

School of Environment and Chemical Engineering, Nanchang Hangkong University, Nanchang, PR China

(*Received 25 October 2013; accepted 31 January 2014*)

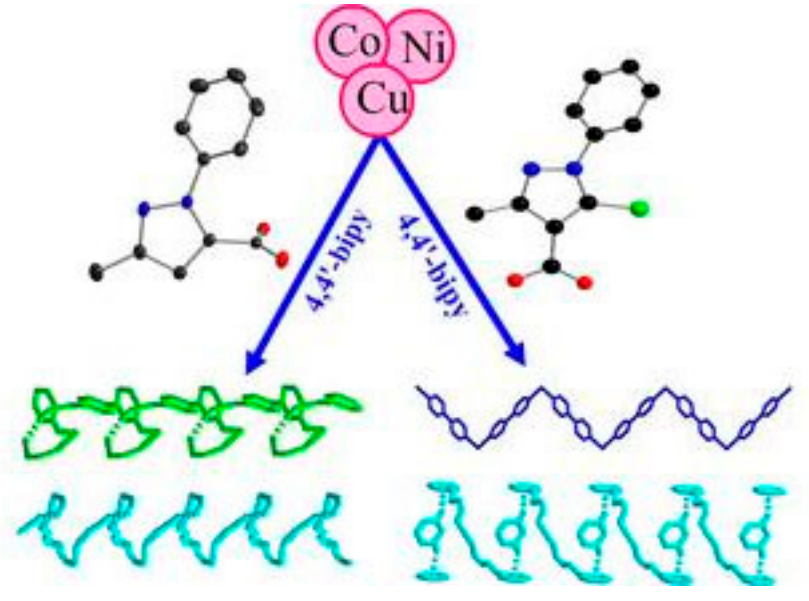

Six new metal complexes with two kinds of phenyl substituted pyrazole carboxylic acid, $[Co(L^1)_2(4,4'\text{-bipy})(H_2O)_2]_n$ (**1**), $[Ni(L^1)_2(4,4'\text{-bipy})(H_2O)_2]_n$ (**2**), $[Cu(L^1)_2(4,4'\text{-bipy})(H_2O)_2]_n$ (**3**), $[Co(L^2)_2(4,4'\text{-bipy})(H_2O)]_n$ (**4**), $[Ni(L^2)_2(4,4'\text{-bipy})(H_2O)]_n$ (**5**), and $[Cu(L^2)_2(4,4'\text{-bipy})]_n$ (**6**) (HL^1 = 3-methyl-1-phenyl-1H-pyrazole-5-carboxylic acid; HL^2 = 5-chloro-3-methyl-1phenyl-1H-pyrazole-4-carboxylic acid; 4,4′-bipy = 4,4′-bipyridine), were prepared and structurally characterized. Complexes **1–6** display 1-D structures and further extend to 3-D supramolecular networks by hydrogen bonding interactions; **1–3** consist of left- and right-handed helical chains and **4–6** contain

*Corresponding author. Email: cbliu@nchu.edu.cn

zig-zag chains. Antibacterial activities of **1–6** against bacteria were studied and compared to the activities of free ligands.

Keywords: Helix; Transition metal complexes; Pyrazole carboxylic acid; N-donor co-ligands; Antibacterial activities

1. Introduction

Design and syntheses of coordination polymers are studied due to their versatile chemical and physical properties and potential applications in catalysis, adsorption, solvent exchange, magnetism, bioactivity, etc. [1–10]. Construction of helical coordination polymers has aroused much attention [11–15] owing to the appearance of helical structures in proteins, collagens, quartz, single-walled carbon nanotubes, and many more natural or artificial fiber-type derivatives [16–20], inspiring scientists to engage in syntheses of artificial helical structures with possible applications in materials sciences, stereoselective catalysis, chemical sensing, and bioactivity [21–26]. A variety of single-, double-, and triple-stranded helical structures have been constructed. However, the structures of complexes depend on combination of several factors, including metal ions, organic ligands, pH, reaction temperature, etc. [27–30], of which ligand is the most important influence, so reasonable selection of ligand is key for achieving this target. Carboxylate with different coordination modes has been extensively used for constructing polynuclear clusters, especially pyrazole carboxylic acid ligands have received much attention owing to some interesting features: they have multiple O- and N-coordination sites together with hydrogen bond acceptors and donors for the assembly of high-dimensional 3d, 4f or 3d–4f supramolecular networks; an appropriate angle between O- and N-coordination sites will provide the potential for formation of helices and/or microporous structures. A phenyl introduced to the pyrazole carboxylic acid enlarges the ligand, increases the possibility of π–π and C–H$\cdots\pi$ interactions [31, 32], and may induce different conformations of pyrazole carboxylic acid due to geometrical constraints and makes the structures of complexes diverse. Different positions of the carboxylate groups on the pyrazole ring may result in different supramolecular structures. In this paper, we synthesized two phenyl substituted pyrazole carboxylic acids with different positions of carboxylate on the pyrazole ring: 3-methyl-1-phenyl-1H-pyrazole-5-carboxylic acid (HL^1) and 5-chloro-3-methyl-1-phenyl-1H-pyrazole-4-carboxylic acid (HL^2). Metal ions due to their different radii and coordination geometries, and auxiliary ligands due to their different sizes and coordination modes, often have significant effects on the formation and structures of complexes [33–35]. In particular, 4,4′-bipy as a linear bridging auxiliary plays a crucial role in the advancement of coordination polymers [36, 37]. Herein, we report syntheses and structures of six new transition metal complexes with two kinds of phenyl substituted pyrazole carboxylic acids and 4,4′-bipy: $[Co(L^1)_2(4,4'\text{-bipy})(H_2O)_2]_n$ (**1**), $[Ni(L^1)_2(4,4'\text{-bipy})(H_2O)_2]_n$ (**2**), $[Cu(L^1)_2(4,4'\text{-bipy})(H_2O)_2]_n$ (**3**), $[Co(L^2)_2(4,4'\text{-bipy})(H_2O)]_n$ (**4**), $[Ni(L^2)_2(4,4'\text{-bipy})(H_2O)]_n$ (**5**), and $[Cu(L^2)_2(4,4'\text{-bipy})]_n$ (**6**), which display helical character through hydrogen bonding interactions.

2. Experimental

2.1. *Materials and instrumentation*

All reagents, except HL^1 and HL^2, were commercially available and used without purification. ^1H NMR spectra were recorded at 400 MHz on a Bruker WH400 DS spectrometer. The elemental analyses of C, H, and N were carried out with a Flash EA 1112 Elementar analyzer. IR spectra were recorded with a Nicolet Avatar 360 FTIR spectrometer using KBr pellets.

2.2. *Syntheses of HL^1 and HL^2*

HL^1 and HL^2 were prepared according to the literature [38, 39], as shown in scheme 1.

HL^1, yield ca. 77.8%; m.p. 176–179 °C. Anal. Calcd for $C_{11}H_{10}N_2O_2$: C, 65.35; H, 4.95; N, 13.86%. Found: C, 65.10; H, 4.87; N, 13.98%. IR data (KBr pellet, ν/cm^{-1}): 3267 m, 2987 m, 1802 m, 1666 s, 1578 m, 1522 s, 1480 s, 1331 m, 1281 m. ^1H NMR (DMSO-d_6, 400 MHz) δ: 3.39 (s, 3H); 6.55 (m, 1H); 7.45–7.53 (m, 5H); 12.44 (s, 1H).

HL^2, yield ca. 82.1%; m.p. 248–250 °C. Anal. Calcd for $C_{11}H_9ClN_2O_2$: C, 55.83; H, 3.83; N, 11.84%. Found: C, 55.50; H, 3.74; N, 12.04%. IR data (KBr pellet, ν/cm^{-1}): 3077 m, 2984 m, 1706 s, 1541 s, 1509 s, 1491 m, 1395 m, 1292 m, 1126 s, 1000 s. ^1H NMR (DMSO-d_6, 400 MHz) δ: 3.32 (s, 3H); 7.40–7.74 (m, 5H); 12.87 (s, 1H).

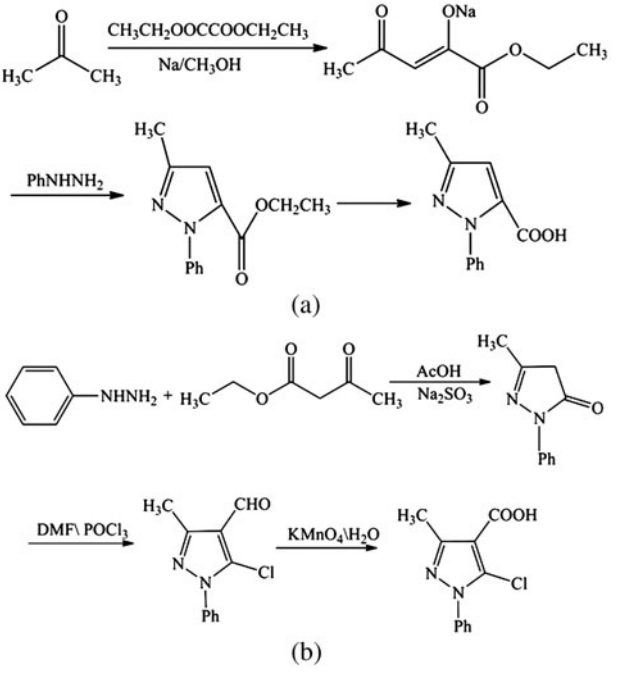

Scheme 1. The synthesis of HL^1 (a) and HL^2 (b).

2.3. *Syntheses of 1–6*

Complexes **1–3** have been produced by reaction of HL^1 and 4,4′-bipy with different transition metal ions, while **4–6** have been obtained by the reaction of HL^2 and 4,4′-bipy with different transition metal ions under hydrothermal conditions.

2.3.1. Synthesis of $[Co(L^1)_2(4,4'\text{-bipy})(H_2O)_2]_n$ (1). A mixture of $CoCl_2{\cdot}6H_2O$ (0.0238 g, 0.1 mM), HL^1 (0.0202 g, 0.1 mM), 4,4′-bipy (0.0156 g, 0.1 mM), NaOH (0.45 mL, 0.65 M L^{-1}), and distilled water (10 mL) were sealed in an undefiled test-tube (20 mL) and heated at 80 °C for 5 h under autogenous pressure. Red block crystals were obtained. Yield: 28.5%. Anal. Calcd for $C_{32}H_{30}CoN_6O_6$: C, 58.81; H, 4.63; N, 12.86%. Found: C, 59.03; H, 4.23; N, 12.98%. IR data (KBr pellet, ν/cm^{-1}): 3156 s, 1609 *versus* 1500 m, 1403 s, 1357 s, 1216 w, 1073 w, 1027 w, 840 m, 787 m, 766 m, 696 m.

2.3.2. Synthesis of $[Ni(L^1)_2(4,4'\text{-bipy})(H_2O)_2]_n$ (2). The synthesis of **2** was the same as that of **1**, except that $Ni(NO_3)_2{\cdot}6H_2O$ was used instead of $CoCl_2{\cdot}6H_2O$. Purple red block crystals were obtained. Yield: 35.5%. Anal. Calcd for $C_{32}H_{30}N_6NiO_6$: C, 58.83; H, 4.63; N, 12.86%. Found: C, 58.94; H, 4.43; N, 13.12%. IR data (KBr pellet, ν/cm^{-1}): 3114 s, 1604 *versus* 1502 m, 1451 m, 1401 s, 1352 s, 1212 w, 1118 w, 1071 w, 1032 w, 838 m, 797 m, 769 m, 696 m.

2.3.3. Synthesis of $[Cu(L^1)_2(4,4'\text{-bipy})(H_2O)_2]_n$ (3). The synthesis of **3** was similar to that of **1**, expect that $CuCl_2{\cdot}5H_2O$ was used instead of $CoCl_2{\cdot}6H_2O$ and the temperature of the reaction mixture was 90 °C. Blue block crystals were obtained. Yield: 34.5%. Anal. Calcd for $C_{32}H_{30}CuN_6O_6$: C, 58.40; H, 4.60; N, 12.77%. Found: C, 57.93; H, 4.83; N, 12.58%. IR data (KBr pellet, ν/cm^{-1}): 3442 s, 3120 s, 1614 *versus* 1501 m, 1400 *versus* 1339 s, 1221 w, 1074 w, 1022 w, 986 w, 817 m, 764 m, 694 m.

2.3.4. Synthesis of $[Co(L^2)_2(4,4'\text{-bipy})(H_2O)]_n$ (4). A mixture of $CoCl_2{\cdot}6H_2O$ (0.0238 g, 0.1 mM), HL^2 (0.0473 g, 0.2 mM), 4,4′-bipy (0.0156 g, 0.1 mM), NaOH (0.3 mL, 0.65 M L^{-1}), and distilled water (10 mL) were sealed in a Teflon-lined stainless reactor (25 mL) and heated at 90 °C for 72 h under autogenous pressure. Cooling to room temperature, the remaining solution was filtered and evaporated slowly at room temperature. Red block crystals were obtained. Yield: 35.5%. Anal. Calcd for $C_{32}H_{26}Cl_2CoN_6O_5$: C, 54.56; H, 3.69; N, 11.93%. Found: C, 54.85; H, 3.36; N, 12.35%. IR data (KBr pellet, ν/cm^{-1}): 3357 w, 3118 w, 1603 m, 1528 s, 1469 m, 1383 s, 1222 m, 1141 m, 1006 m, 809 m, 764 m.

2.3.5. Synthesis of $[Ni(L^2)_2(4,4'\text{-bipy})(H_2O)]_n$ (5). The synthesis of **5** was the same as that of **4**, except that 0.1 mM $NiCl_2{\cdot}6H_2O$ was used instead of 0.1 mM $CoCl_2{\cdot}6H_2O$ and the temperature was increased to 120 °C. Green block crystals were obtained. Yield: 31.5%. Anal. Calcd for $C_{32}H_{26}Cl_2NiN_6O_5$: C, 54.58; H, 3.69; N, 11.96%. Found: C, 54.92; H, 3.32; N, 12.25%. IR data (KBr pellet, ν/cm^{-1}): 3371 w, 3129 w, 1601 m, 1536 s, 1468 m, 1386 s, 1231 m, 1141 m, 1006 m, 764 m.

2.3.6. Synthesis of $[Cu(L^2)_2(4,4'\text{-bipy})]_n$ (6). The synthesis of **6** was the same as that of **5**, except that $CuSO_4 \cdot 5H_2O$ (0.1 mM, 0.027 g) was used instead of 0.1 mM $NiCl_2 \cdot 6H_2O$. Blue columnar crystals were obtained. Yield: 37.5%. Anal. Calcd for $C_{32}H_{24}Cl_2CuN_6O_4$: C, 55.62; H, 3.47; N, 12.16%. Found: C, 55.95; H, 3.25; N, 12.42%. IR data (KBr pellet, ν/cm^{-1}): 3434 m, 2926 w, 1610 *versus* 1523 m, 1470 s, 1376 s, 1348 m, 1218 m, 1134 m, 1004 w, 771 m.

2.4. *X-ray crystallographic study*

X-ray single-crystal data of **1–6** were recorded on a Bruker APEX II area detector diffractometer with graphite-monochromated Mo-Kα radiation ($\lambda = 0.71073$ Å). Semi-empirical absorption corrections were applied to **1–6** using SADABS [40]. The structures were solved by direct methods [41] and refined by full-matrix least squares on F^2 using SHELXL-97 [42]. All non-hydrogen atoms were refined anisotropically. The carboxyl and water hydrogens were located from difference Fourier maps; the other hydrogens were placed in geometrically calculated positions. Experimental details for X-ray data collection of **1–6** are presented in table 1 and selected bond lengths are listed in table 2; the main hydrogen bonding lengths and angles are listed in table 3.

2.5. *Antibacterial testing*

The *in vitro* antibacterial activities of HL^1, HL^2, and **1–6** were tested against gram positive bacteria, *Staphylococcus aureus*, *Candida albicans* and *Bacillus subtilis*, and Gram-negative bacteria, *Escherichia coli* and *Pseudomonas aeruginosa*, by the minimum inhibitory concentration (MIC) method. The compounds were dissolved in DMF with two-fold serial dilutions from 200 to 6.25 μg mL^{-1}. Sterile microtubes were filled with 1 mL of serial two-fold dilutions of the compounds. A growth tube (broth plus inoculum) and a sterility control tube (broth only) were included each time. The tubes were incubated at 37 °C for 24 h. MICs were defined as the lowest concentrations of the compounds which inhibited the growth of micro-organisms; DMF was inactive under the applied conditions.

3. Results and discussion

3.1. *Description of the structures*

3.1.1. Crystal structure of $[Co(L^1)_2(4,4'\text{-bipy})(H_2O)_2]_n$ (1). Crystallographic analysis revealed that **1–3** are isostructural. The asymmetric unit of **1** contains a half Co(II), one L^1, one water, and a half 4,4′-bipy. Co(II) in **1** coordinates to two carboxyl oxygens from two L^1, two nitrogens from two 4,4′-bipy molecules, and another two oxygens from two waters as shown in figure 1, displaying a distorted octahedral geometry. In **1**, L^1 is monodentate (see scheme 2(a)), having two orientations with the dihedral angle of 21.90° between the pyrazole rings in **1**. The carboxylates are out of the planes of pyrazole rings with dihedral angle of 63.29° and the phenyl and pyrazole rings of L^1 ligands in **1** are twisted by an angle of 46.25°. The 4,4′-bipy molecules are bis(monodentate) bridges, linking Co(II) ions into a

Table 1. Crystal data for **1–6**.

Complex	**1**	**2**	**3**	**4**	**5**	**6**
Empirical formula	$C_{32}H_{30}CoN_6O_6$	$C_{32}H_{30}N_6NiO_6$	$C_{32}H_{30}CuN_6O_6$	$C_{32}H_{26}Cl_2CoN_6O_5$	$C_{32}H_{26}Cl_2NiN_6O_5$	$C_{32}H_{24}Cl_2CuN_6O_4$
Formula weight	653.55	653.33	658.16	704.42	704.20	691.01
T (K)	296(2)	273(2)	296(2)	296(2)	296(2)	296(2)
Crystal system	Monoclinic	Monoclinic	Monoclinic	Triclinic	Triclinic	Orthorhombic
Space group	*C2/c*	*C2/c*	*C2/c*	$P\bar{1}$	$P\bar{1}$	*Fdd2*
a/Å	17.851(17)	17.824(17)	18.716(14)	7.863(4)	7.857(8)	21.415(11)
b/Å	11.452(11)	11.296(11)	11.151(8)	14.799(8)	14.738(15)	25.177(13)
c/Å	16.780(16)	16.653(16)	15.296(11)	15.581(8)	15.477(15)	11.123(6)
α/°	90	90	90	61.650(10)	61.869(10)	90
β/°	115.132(10)	115.129(13)	110.939(10)	79.297(10)	86.275(10)	90
γ/°	90	90	90	74.744(10)	75.029(10)	90
V/Å^3	3105.4(5)	3036.0(5)	2981.4(4)	1535.3(14)	1523.5(3)	5997.3(5)
Z	4	4	4	2	2	8
Crystal size (mm)	0.37 × 0.35 × 0.21	0.43 × 0.27 × 0.10	0.48 × 0.35 × 0.12	0.47 × 0.44 × 0.18	0.21 × 0.17 × 0.15	0.22 × 0.11 × 0.09
D_c (mg m^{-3})	1.398	1.430	1.466	1.524	1.535	1.531
μ (mm^{-1})	0.607	0.694	0.789	0.786	0.865	0.956
F (0 0 0)	1356	1360	1364	722	724	2824
θ range (°)	2.52–25.50	2.70–25.50	2.35–25.49	2.67–25.50	2.65–25.50	2.22–27.50
Goodness-of-fit on F^2 (e Å^{-3})	1.078	1.020	1.048	1.027	0.986	1.031
No. data collected	11,250	11,443	11,204	11,892	11,992	13,236
No. unique data	2889	2830	2772	5689	5650	3429
Rint	0.0188	0.0174	0.0170	0.0136	0.0158	0.0232
$R1$, $wR2$ [$I > 2\sigma(I)$]	0.0309, 0.0846	0.0268, 0.0709	0.0267, 0.0709	0.0319, 0.0803	0.0334, 0.0685	0.0229, 0.0575
$R1$, $wR2$ (all data)	0.0353, 0.0902	0.0310, 0.0745	0.0295, 0.0729	0.0368, 0.0847	0.0422, 0.0727	0.0257, 0.0587
Largest diff. peak and hole (e Å^{-3})	0.414, −0.599	0.270, −0.192	0.268, −0.295	0.467, −0.585	0.438, −0.498	0.239, −0.188

Table 2. Selected bond lengths (Å) for **1–6**.

1			
Co(1)–O(3)	2.083(13)	Co(1)–O(3)#1	2.083(13)
Co(1)–O(2)	2.092(12)	Co(1)–O(2)#1	2.092(12)
Co(1)–N(3)	2.170(2)	Co(1)–N(4)#2	2.200(2)
2			
Ni(1)–O(3)	2.049(2)	Ni(1)–O(3)#1	2.049(2)
Ni(1)–O(2)	2.051(2)	Ni(1)–O(2)#1	2.052(2)
Ni(1)–N(3)	2.133(3)	Ni(1)–N(4)#2	2.107(3)
3			
Cu(1)–O(2)#1	1.955(12)	Cu(1)–O(3)	2.418(14)
Cu(1)–O(2)	1.955(12)	Cu(1)–O(3)#1	2.418(14)
Cu(1)–N(3)	2.035(18)	Cu(1)–N(4)#2	2.049(18)
4			
Co(1)–O(1)	2.079(14)	Co(1)–O(5)	2.103(16)
Co(1)–O(3)	2.187(15)	Co(1)–N(5)	2.163(16)
Co(1)–O(4)	2.128(15)	Co(1)–N(6)	2.155(17)
5			
Ni(1)–O(1)	2.065(15)	Ni(1)–O(5)	2.069(17)
Ni(1)–O(3)	2.116(16)	Ni(1)–N(5)	2.114(19)
Ni(1)–O(4)	2.125(15)	Ni(1)–N(6)	2.092(18)
6			
Cu(1)–O(1)	2.769(15)	Cu(1)–O(1)#3	2.769(15)
Cu(1)–O(2)	1.925(11)	Cu(1)–O(2)#3	1.925(11)
Cu(1)–N(3)	2.018(2)	Cu(1)–N(4)#4	2.029(2)

Note: Symmetry operations: #1 $-x+2, y, -z+1/2$; #2 $x, y+1, z$; #3 $-x, -y, z$; #4 $x, y, -1+z$.

1-D chain (figure 2), and the dihedral angle between the pyridine rings is 50.17°. In **1**, there are abundant hydrogen bonds: (a) between coordinated water and carboxyl oxygen; (b) between nitrogen of pyrazole and coordinated water; (c) between C–H of phenyl or pyridine rings and carboxyl oxygen (table 3), which extend 1-D chains into a 3-D supramolecular network consisting of left- and right-handed helical chains (figure 3); the pitch of the helix is the same as the length of the *b* axis (11.30 Å).

3.1.2. Crystal structure of $[Cu(L^1)_2(4,4'\text{-bipy})(H_2O)_2]_n$ (3). Although **1–3** are isostructural, the asymmetric unit of **3** is similar to **1** and **2**, but L^1 in **3** have different orientations compared to those in **1** and **2**. The dihedral angle between the pyrazole rings in **3** is 56.57°. Carboxylates are out of the planes of pyrazole rings with dihedral angle of 37.86°, and the phenyl and pyrazole rings of L^1 in **3** are twisted by an angle of 51.75°. Each Cu(II) is bridged by 4,4′-bipy with dihedral angle between pyridine rings of 52.66°, giving a 1-D chain structure, and the 1-D chains are further extended into a 3-D supramolecular network via O–H···N, O–H···O, and C–H···O hydrogen bonds, of which O3–H2···N2 and C3–H3···O1 link Cu(II) ions forming left- and right-handed helical chains, and the pitch of the helix is the same as the length of the *b* axis (11.15 Å), as shown in figure 4.

Table 3. Hydrogen bonding geometry (Å and °) for **1–6**.

D–H•A	d(D–H)	d(H…A)	d(D…A)	∠(DHA)
1				
O(3)–H(1W)···O(1)	0.82	2.01	2.750(19)	149.0
O(3)–H(2W)···N(2)#1	0.79	2.01	2.794(2)	173.0
C(3)–H(3)···O(1)#2	0.93	2.59	3.445(2)	154.0
C(7)–H(7)···O(2)#3	0.93	2.50	3.416(3)	170.0
C(10)–H(10)···O(1)#4	0.93	2.50	3.339(3)	150.0
C(12)–H(12)···O(2)	0.93	2.44	3.052(2)	124.0
C(17)–H(17)···O(1)#5	0.93	2.58	3.401(2)	147.0
2				
O(3)–H(2 W)···O(1)	0.82	1.99	2.728(3)	149.0
O(3)–H(1 W)···N(2)#1	0.83	1.97	2.795(3)	174.0
C(3)–H(3)···O(1)#2	0.93	2.56	3.423(4)	154.0
C(7)–H(7)···O(2)#3	0.93	2.44	3.362(4)	170.0
C(10)–H(10)···O(1)#4	0.93	2.45	3.294(4)	150.0
C(12)–H(12)···O(1)	0.93	2.56	3.368(4)	146.0
C(17)–H(17)···O(2)#5	0.93	2.38	2.992(4)	123.0
3				
O(3)–H(2 W)···N(2)#1	0.85	2.12	2.942(2)	164.0
C(3)–H(3)···O(1)#2	0.93	2.58	3.450(3)	155.0
C(12)–H(12)···O(3)#3	0.93	2.45	3.140(2)	131.0
O(3)–H(1 W)···O(1)	0.82	2.10	2.751(2)	136.0
4				
O(5)–H(1 W)···N(4)#1	0.83	2.07	2.880(3)	166.0
O(5)–H(2 W)···O(2)	0.83	1.72	2.504(3)	157.0
C(17)–H(17)···O(5)#1	0.93	2.55	3.217(4)	129.0
C(21)–H(21B)···O(3)	0.96	2.60	3.117(3)	114.0
C(23)–H(23)···Cl(1)	0.93	2.61	3.436(3)	149.0
C(23)–H(23)···O(1)	0.93	2.35	2.992(3)	126.0
C(15)–H(15)···π#2	0.93	2.85	3.575(5)	136.0
5				
O(5)–H(1 W)···N(4)#1	0.83	2.10	2.903(3)	163.0
O(5)–H(2 W)···O(2)	0.83	1.70	2.502(4)	161.0
C(17)–H(17)···O(5)#1	0.93	2.52	3.188(4)	129.0
C(21)–H(21B)···O(4)	0.96	2.58	3.113(4)	115.0
C(23)–H(23)···Cl(1)	0.93	2.60	3.417(3)	146.0
C(23)–H(23)···O(1)	0.93	2.30	2.937(3)	125.0
C(15)–H(15)···π#2	0.93	2.84	3.574(5)	136.0
6				
C(12)–H(12)···O(2)	0.93	2.35	2.900(2)	117.0
C(16)–H(16)···π#1	0.93	2.71	3.536(2)	149.0

Note: Symmetry codes: for **1**: #1 $x+1/2, -y+1/2, z+1/2$; #2 $-x+2, -y+1, -z$; #3 $-x+3/2, -y+1/2, -z$; #4 $-x+2, -y, -z$; #5 $x, y-1, z$; for **2**: #1 $x+1/2, -y+3/2, z+1/2$; #2 $-x+2, -y+1, -z$; #3 $-x+3/2, -y+3/2, -z$; #4 $-x+2, -y+2, -z$; #5 $x, y-1, z$; for **3**: #1 $x+1/2, -y+1/2, z+1/2$; #2 $-x+2, -y+1, -z$; #3 $-x+2, y, -z+1/2$; for **4**: #1 $-x+1, -y, -z+1$; #2 $x, y-1, z+1$; for **5**: #1 $-x+1, -y+1, -z$; #2 $x, y, z-1$; for **6**: #1 $x-1/4, -y+1/4, z+3/4$.

3.1.3. Crystal structure of $[Co(L^2)_2(4,4'\text{-bipy})(H_2O)]_n$ (4). Crystallographic analysis revealed that **4** and **5** are isostructural, so only the crystal structure of **4** is described here in detail. The asymmetric unit of **4** contains one Co(II), two L^2, one 4,4′-bipy, and one water. As shown in figure 5, in **4**, Co(II) coordinates to three carboxylate oxygens from two L^2, one oxygen from a water, and another two nitrogens from two 4,4′-bipy molecules in a distorted octahedral geometry. The L^2 adopt two kinds of coordination modes in **4**, one monodentate and the other chelating–bidentate (see scheme 3(b) and (c)). For convenience,

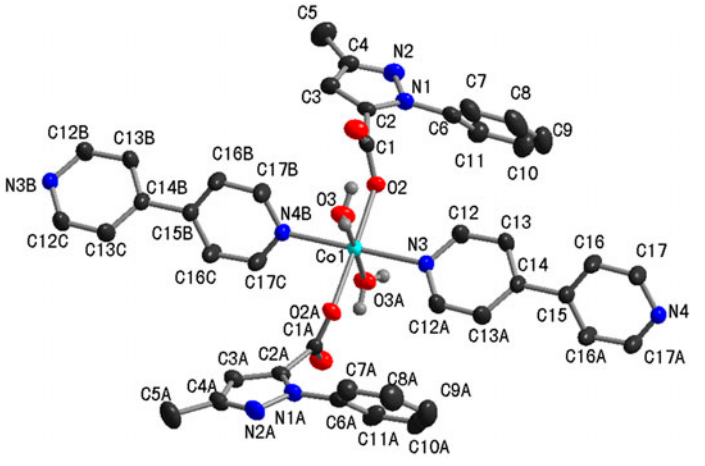

Figure 1. Coordination environment of Co(II) in **1** with 30% thermal ellipsoids.

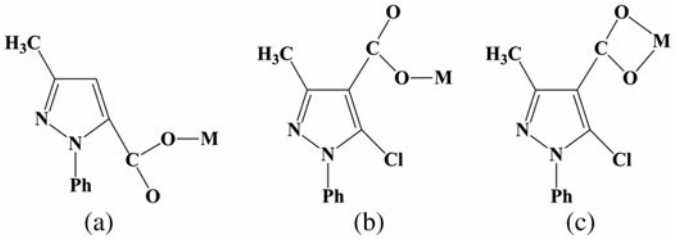

Scheme 2. The coordination modes of HL^1 and HL^2 in **1–6**.

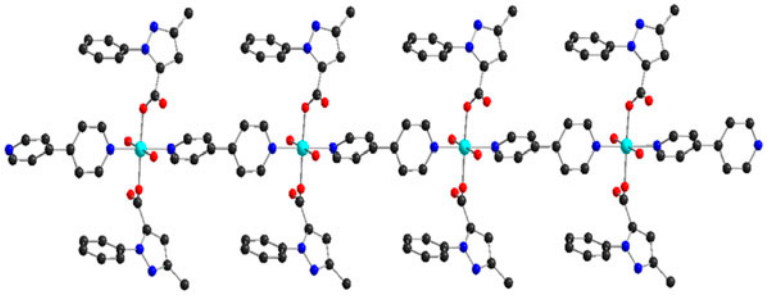

Figure 2. 1-D chain structure of **1** with 30% thermal ellipsoids.

the monodentate ligand is named as L^{2a} and the chelating–bidentate ligand is named as L^{2b}. The dihedral angle between the phenyl and pyrazole rings in L^{2a} and L^{2b} are 60.10° and 50.82°, respectively, and that between the pyrazole rings of L^{2a} and L^{2b} is 84.36°. In **4**, 4,4′-bipy is bis(monodentate) bridging with dihedral angle of 87.99° between pyridine rings, linking Co(II) ions into a 1-D zig-zag chain (figure 6). The 1-D chain structures are further connected into a 3-D supramolecular network (figure 7) via hydrogen bonds and C–H$\cdots\pi$ interactions (H$\cdots\pi$ distance is 2.85 Å and C–H$\cdots\pi$ angle is 136°).

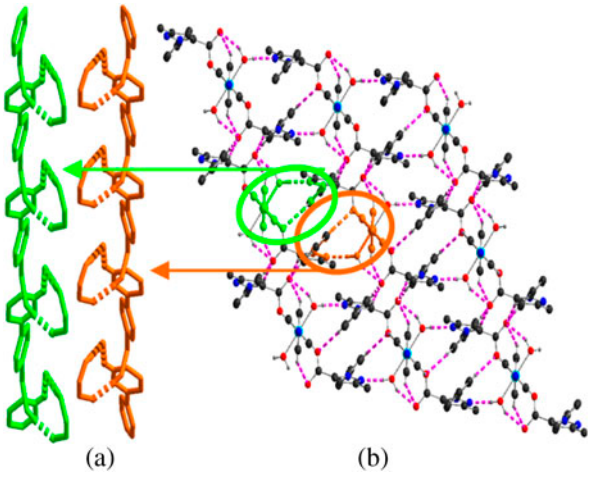

Figure 3. (a) View of helical chains with left-handed (green) and right-handed (orange) helices in **1** along the *c* axis. (b) The 3-D supramolecular network of **1** along the *b* axis (see http://dx.doi.org/10.1080/00958972.2014.896993 for color version).

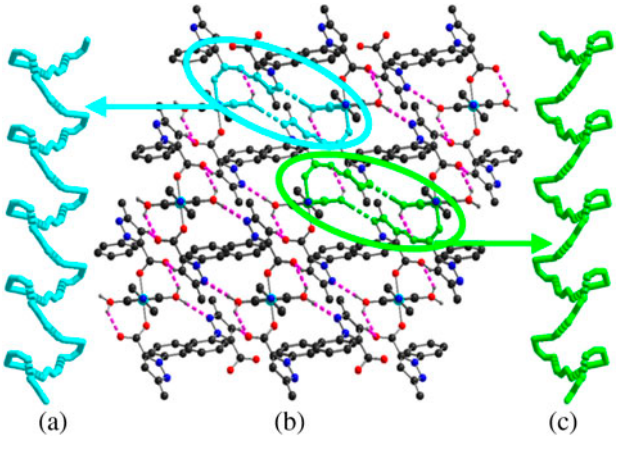

Figure 4. (a) The 3-D supramolecular network of **3** along the *b* axis. (b) View of helical chains with left-handed (blue) helices. (c) Right-handed (green) helices in **3** along the *c* axis (see http://dx.doi.org/10.1080/00958972.2014.896993 for color version).

3.1.4. Crystal structure of $[Cu(L^2)_2(4,4'\text{-bipy})]_n$ (6). The asymmetric unit in **6** consists of a half copper(II), one L^2, and a half 4,4′-bipy. As shown in figure 8, the Cu(II) in **6** is six-coordinate with four oxygens from two L^2 and two nitrogens from two 4,4′-bipy molecules. Cu(II) is coplanar with N3, N4B, O1, and O1A. Two pyridine nitrogens N3, N4B and two carboxylate oxygens O2, O2A reside in equatorial positions with bond lengths varying from 1.925(11) to 2.029(2) Å, while axial positions are occupied by O1 and O1A, axial Cu–O bond lengths are 2.769(15) Å, and the axial bond angle is 156.47(44)°. Cu(II) ions locate in an elongated octahedral environment because of the Jahn–Teller effect. Different from **4**, in **6**, L^2 only display chelating–bidentate mode; the phenyl and pyrazole rings

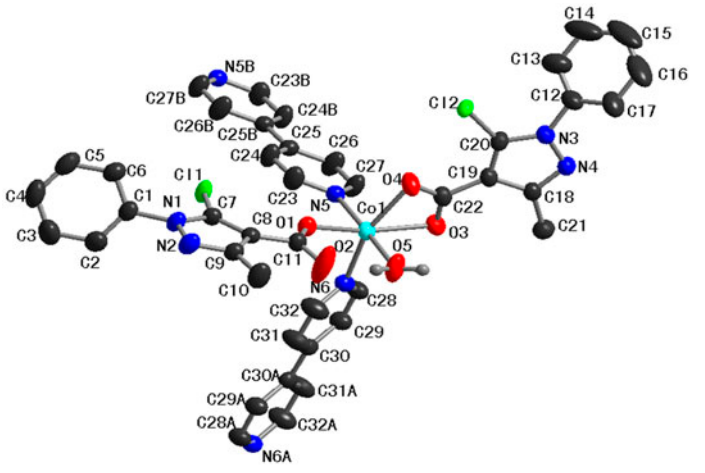

Figure 5. Coordination environment of Co(II) in **4** with 30% thermal ellipsoids.

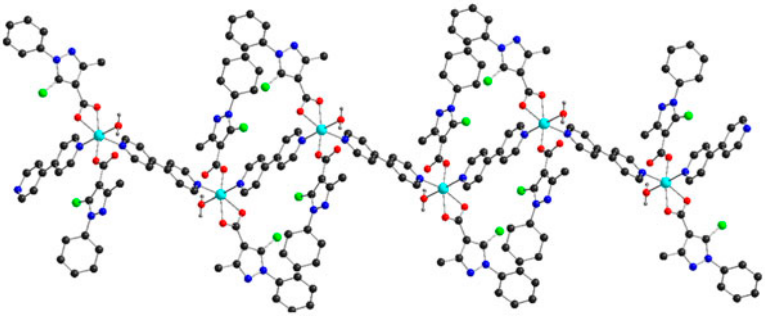

Figure 6. The 1-D zig-zag chain structure of **4** formed by 4,4′-bipy.

of L^2 are twisted by an angle of 58.47°. 4,4′-Bipy in which pyridine rings are coplanar are bis(monodentate) bridges, linking Cu(II) ions into a 1-D chain (figure 9), and the 1-D chains are further stacked to a 3-D supramolecular network (figure 10) along the *c* axis via C–H···π interactions between C–H groups of 4,4′-bipy and phenyl rings of L^2 (H···π distance is 2.71 Å and C–H···π angle is 149°). The [Cu(L^2)$_2$(4,4′-bipy)] monomers are joined into a zig-zag chain through C(16)–H(16)···π interaction, as shown in figure 11.

3.2. *Comparison of the structures*

The positions of carboxylate on the pyrazole ring for HL^1 and HL^2 are different, and HL^2 contains one more chlorine substituent. L^1 and L^2 display different coordination modes in **1–6** (scheme 2), but the structures of corresponding complexes with L^1 and L^2 are very similar. The coordination numbers of **1–6** all are six, and **1–3** with L^1 and **4–6** with L^2 all display 1-D structures connected by 4,4′-bipy. All are extended to 3-D supramolecular networks via hydrogen bonding interactions, as shown in scheme 3. Complexes **1–3** with L^1 are helical chains, while helical chains are not observed in **4–6** with L^2, showing that the position of carboxylate has an effect on formation of the helix.

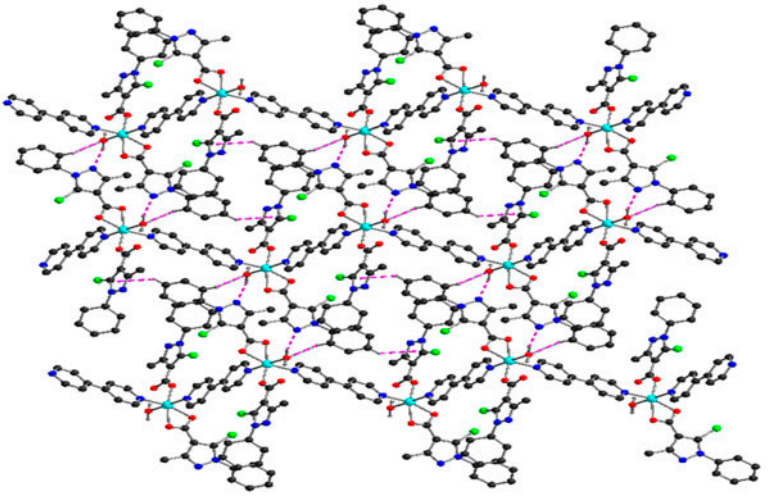

Figure 7. The 3-D supramolecular network of **4** along the *a* axis.

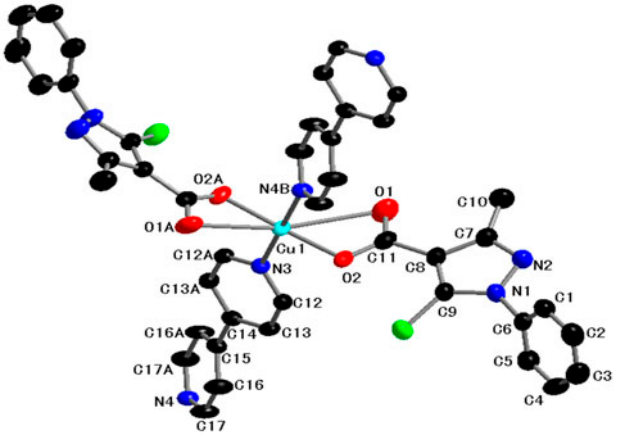

Figure 8. Coordination environment of Cu(II) in **6** with 30% thermal ellipsoids.

For the same ligand, **1–3** and **4** and **5** are isostructural because Co(II), Ni(II), and Cu(II) ion radii are very close. In **1–3**, L^1 are monodentate with two orientations. The dihedral angles between the planes of pyrazole ring are 21.90°, 22.50°, and 56.57° in **1–3**, respectively; the phenyl and pyrazole rings of L^1 are twisted by an angle of 46.25°, 46.06°, and 51.75° in **1–3**, respectively, and the dihedral angles between the pyrazole rings and the carboxylates are 63.30°, 64.73°, and 37.86° in **1–3**, respectively. L^2 have two kinds of coordination modes: monodentate and chelating–bidentate in **4** and **5**, but only chelating–bidentate in **6**. L^2 have different orientations in **4–6**. The dihedral angles between the planes of pyrazole ring are 84.36°, 85.92°, and 64.92° in **4–6**, respectively; the phenyl and pyrazole rings of chelating–bidentate ligand are twisted by angles of 50.82°, 51.36°, and 58.47° in **4–6**, respectively, and that of monodentate ligand are twisted by angles of 60.10° and

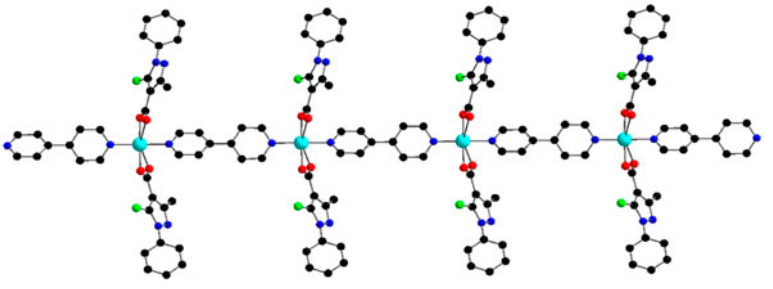

Figure 9. The 1-D chain structure of **6** with 30% thermal ellipsoids.

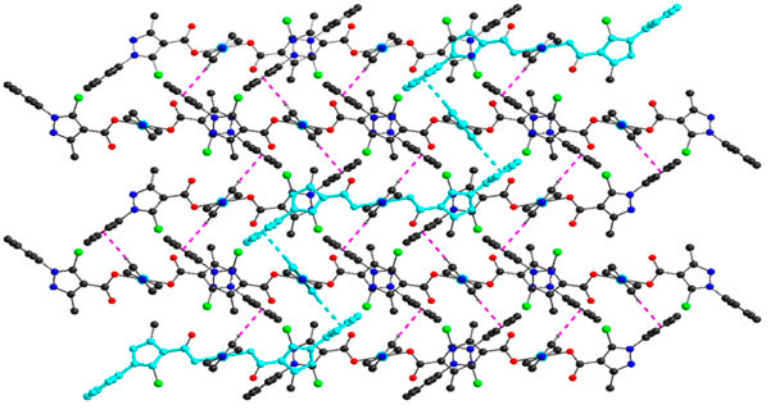

Figure 10. The 3-D supramolecular network of **6** along the *c* axis.

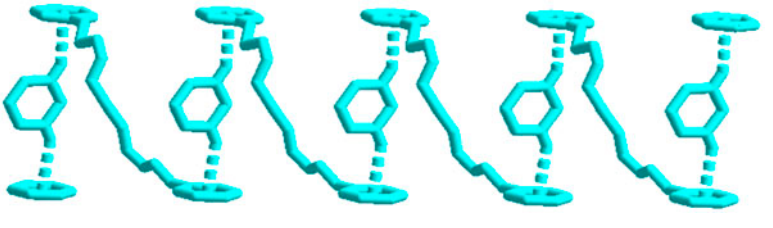

Figure 11. The zig-zag chain of **6** through C–H$\cdots\pi$ interaction along the *c* axis.

60.76° in **4** and **5**, respectively. Dihedral angles between the pyrazole rings and carboxylates of chelating–bidentate ligands are 17.25°, 17.18°, and 13.86° in **4**–**6**, respectively, and that of monodentate ligand are 9.35° and 8.65° in **4** and **5**, respectively. 4,4′-Bipy molecules have different orientations in **1**–**6** with dihedral angles between pyridine rings of 50.17°, 51.64°, 52.66°, 87.99°, and 89.55° in **1**–**5**, respectively, and in **6**, pyridine rings are coplanar. In **4** and **5**, waters coordinate, however, there are no water molecules in **6**, showing that hydrogen bonding interactions between coordinated water and C–H groups of phenyl rings have a significant effect on the structures of **4** and **5**; metal ions can affect the coordination of L^2.

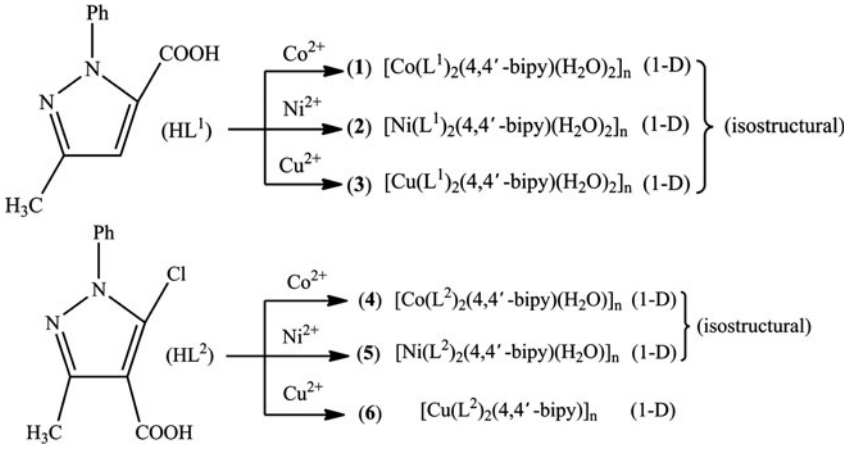

Scheme 3. Schematic procedure and dimensional relationship of metal ions and ligands of **1–6**.

Recently, some coordination polymers based on nitrogen-heterocyclic carboxylate with helical structures have been reported. For example, $[Zn_2(\mu_3\text{-HBuPhIDC})_2(CH_3OH)_2]$ (μ_3-HBuPhIDC = 2-(p-tert-butylphenyl)-1H-imidazole-4,5-dicarboxylic acid) displays an interesting 3-D open architecture, which contains infinite 1-D octagonal channels built by left- and right-handed helical chains [43]. $[Co(L)_2(H_2O)_2]_n \cdot 2nH_2O$ and $[Ni(L)_2(H_2O)_2]_n \cdot 2nH_2O$ (HL = 2-(6-oxo-6H-purin-1(9H)-yl)acetic acid) show a 2-D structure composed of left- and right-handed metal-organic helices sharing common metal centers [44] with all of the helical chains formed via coordination bonds. However, **1–3** exhibit 1-D structures and the helical chains formed via coordination bonds as well as hydrogen bonds.

3.3. *Antibacterial activity results*

The antibacterial activities of HL^1, HL^2, and **1–6** have been measured against selected micro-organisms. From the results given in table 4, ligands show antibacterial activities against the Gram-positive bacteria *S. aureus*, *C. albicans,* and *B. subtilis*, and Gram-negative bacteria *E. coli* and *P. aeruginosa I*, with MIC values between 25 and 100 μg mL^{-1}, while MIC values of the complexes are between 6.25 and 25 μg mL^{-1}. The MIC values of

Table 4. MIC values of HL^1, HL^2, and **1–6** against the tested bacteria (μg mL^{-1}).

Compounds	*S. aureus*	*C. albicans*	*B. subtilis*	*E. coli*	*P. aeruginosa*
HL^1	50	50	100	100	50
HL^2	25	25	50	25	25
4,4′-bipy	25	50	50	100	50
1	25	12.5	25	25	25
2	25	12.5	12.5	25	25
3	25	25	12.5	25	25
4	12.5	12.5	25	25	12.5
5	12.5	6.25	6.25	25	12.5
6	12.5	25	6.25	12.5	6.25

1–6 are lower than that of HL^1 and HL^2, indicating that the antibacterial activities of metal complexes are better than those of corresponding free ligands against the tested bacteria. For *S. aureus* and *P. aeruginosa*, **4–6** with L^2 show better antibacterial activities than **1–3** with L^1, while for the other bacteria, **4–6** show the same antibacterial activities as **1–3**, and some show better antibacterial activities than **1–3**.

4. Conclusion

Six new transition metal coordination polymers with two kinds of phenyl substituted pyrazole carboxylic acids have been obtained and characterized. Complexes **1–6** all display 1-D structures connected by 4,4′-bipy, and all extended to 3-D supramolecular networks via hydrogen bonding interactions and other weak intermolecular interactions. Complexes **1–3** comprise single-stranded helices, while **4–6** contain zig-zag chains. Single-crystal X-ray diffraction results show that variation of the carboxylate group position lead to different structures of complexes. Metal ions, hydrogen bonds, bridging conformations of carboxylates, and N-donor co-ligands have significant influence on the helical structures of **1–6**. Antibacterial measurements show that the inhibitory effect of the complexes is stronger than those of corresponding free ligands.

Supplementary material

CCDC 933049-933054 contain the supplementary crystallographic data for **1–6**. These data can be obtained free of charge via http://www.ccdc.cam.ac.uk/conts/retrieving.html, or from the Cambridge Crystallographic Data Center, 12 Union Road, Cambridge CB2 1EZ, UK; Fax: (+44)1223-336-033; or E-mail: deposit@ccdc.cam.ac.uk.

Funding

This work was supported by the Natural Science Foundation of China [grant number 21264011], [grant number 20961007]; the Aviation Fund [grant number 2010ZF56023] and the Young Scientists Program of Jiangxi Province [grant number 2008DQ00600].

References

[1] P.M. Forster, D.S. Kim, A.K. Cheetham. *Solid State Sci.*, **7**, 594 (2005).
[2] B. Chen, L. Wang, Y. Xiao, F.R. Fronczek, M. Xue, Y. Cui, G. Qian. *Angew. Chem. Int. Ed.*, **48**, 500 (2009).
[3] J.B. Lin, J.P. Zhang, X.M. Chen. *J. Am. Chem. Soc.*, **132**, 6654 (2010).
[4] D. Zhao, D.J. Timmons, D. Yuan, H.C. Zhou. *Acc. Chem. Res.*, **44**, 123 (2010).
[5] J.S. Miller, D. Gatteschi. *Chem. Soc. Rev.*, **40**, 3065 (2011).
[6] M.D. Allendorf, C.A. Bauer, R.K. Bhakta, R.J.T. Houk. *Chem. Soc. Rev.*, **38**, 1330 (2009).
[7] M. Kurmoo. *Chem. Soc. Rev.*, **38**, 1353 (2009).
[8] L. Ma, C.D. Wu, M.M. Wanderley, W. Lin. *Angew. Chem. Int. Ed.*, **49**, 8244 (2010).

[9] Z.H. Shen, D.F. Xu, N.N. Cheng, X.N. Zhou, X.K. Chen, Y.H. Xu, Q.Z. He. *J. Coord. Chem.*, **64**, 2342 (2011).
[10] A. Tăbăcaru, C. Pettinari, F. Marchetti, C. di Nicola, K.V. Domasevitch, S. Galli, N. Masciocchi, S. Scuri, I. Grappasonni, M. Cocchioni. *Inorg. Chem.*, **51**, 9775 (2012).
[11] L. Han, M.C. Hong. *Inorg. Chem. Commun.*, **8**, 406 (2005).
[12] L.F. Ma, L.Y. Wang, X.K. Huo, Y.Y. Wang, Y.T. Fan, J.G. Wang, S.H. Chen. *Cryst. Growth Des.*, **8**, 620 (2008).
[13] E. Yang, J. Zhang, Z.J. Li, S. Gao, Y. Kang, Y.B. Chen, Y.H. Wen, Y.G. Yao. *Inorg. Chem.*, **43**, 6525 (2004).
[14] H. Imai, K. Inoue, K. Kikuchi, Y. Yoshida, M. Ito, T. Sunahara, S. Onaka. *Angew. Chem. Int. Ed.*, **43**, 5618 (2004).
[15] V. Urban, T. Pretsch, H. Hartl. *Angew. Chem. Int. Ed.*, **44**, 2794 (2005).
[16] N. Sewald, H.D. Jakubke. *Peptides: Chemistry and Biology*, Wiley-VCH, Weinheim, Germany (2002).
[17] J.H. Jung, Y. Ono, S. Shinkai. *Chem. Eur. J.*, **6**, 4552 (2000).
[18] K.P. Meurer, F. Vögtle. *Top. Curr. Chem.*, **127**, 1 (1985).
[19] J.W. Mintmire, C.T. White. *Phys. Rev. Lett.*, **81**, 2506 (1998).
[20] M. Albrecht. *Angew. Chem. Int. Ed.*, **44**, 6448 (2005).
[21] C. Janiak. *Dalton Trans.*, 2781 (2003).
[22] S.L. James. *Chem. Soc. Rev.*, **32**, 276 (2003).
[23] S. Kitagawa, R. Kitaura, S. Noro. *Angew. Chem. Int. Ed.*, **43**, 2334 (2004).
[24] T. Nakano, Y. Okamoto. *Chem. Rev.*, **101**, 4013 (2001).
[25] X.F. Zhu, Y.H. Fan, Q. Wang, C.L. Chen, M.X. Li, J.W. Zhao, J. Zhou. *Russ. J. Coord. Chem.*, **38**, 478 (2012).
[26] K.B. Wang, X.Y. Ma, D.L. Shao, Z.R. Geng, Z.Y. Zhang, Z.L. Wang. *Cryst. Growth Des.*, **12**, 3786 (2012).
[27] Z. Su, S.S. Chen, J. Fan, M.S. Chen, Y. Zhao, W.Y. Sun. *Cryst. Growth Des.*, **10**, 3675 (2010).
[28] Z. Su, K. Cai, J. Fan, S.S. Chen, M.S. Chen, W.Y. Sun. *CrystEngComm.*, **12**, 100 (2010).
[29] Q.R. Fang, G.S. Zhu, M. Xue, Z.P. Wang, J.Y. Sun, S.L. Qiu. *Cryst. Growth Des.*, **8**, 319 (2008).
[30] W.J. Zhuang, X.J. Zheng, L.C. Li, D.Z. Liao, H. Ma, L.P. Jin. *CrystEngComm.*, **9**, 653 (2007).
[31] S.Y. Wan, Y.T. Huang, Y.Z. Li, W.Y. Sun. *Microporous Mesoporous Mater*, **73**, 101 (2004).
[32] Q. Shi, Y.T. Sun, L.Z. Sheng, K.F. Ma, X.Q. Cai, D.S. Liu. *Inorg. Chim. Acta*, **362**, 4167 (2009).
[33] Q. Chu, G.X. Liu, Y.Q. Huang, X.F. Wang, W.Y. Sun. *Dalton Trans.*, 4302 (2007).
[34] J.P. Zhang, S. Kitagawa. *J. Am. Chem. Soc.*, **130**, 907 (2008).
[35] P. Kanoo, T.K. Maji. *Eur. J. Inorg. Chem.*, **24**, 3762 (2010).
[36] D.L. Reger, J.J. Horger, M.D. Smith, G.J. Long, F. Grandjean. *Inorg. Chem.*, **50**, 686 (2011).
[37] F. Costantino, A. Ienco, S. Midollini, A. Orlandini, A. Rossin, L. Sorace. *Eur. J. Inorg. Chem.*, **20**, 3179 (2010).
[38] B.A. Tertov, A.S. Morkovnik. *Khim. Geterotsikl. Soedin.*, **3**, 392 (1975).
[39] M. Abdel-Azzem, M. Zahran. *Bull. Chem. Soc. Jpn.*, **67**, 1879 (1994).
[40] G.M. Sheldrick. *SADABS, Program for Empirical Absorption Correction of the Area Detector Data*, University of Göttingen, Germany (1997).
[41] G.M. Sheldrick. *SHELXS-97, Program for Crystal Structure Solution*, University of Göttingen, Germany (1997).
[42] G.M. Sheldrick. *SHELXL-97, Program for Crystal Structure Refinement*, University of Göttingen, Germany (1997).
[43] F.J. Yin, H. Zhao, X.Y. Xu, M.W. Guo. *J. Coord. Chem.*, **66**, 3199 (2013).
[44] X.Q. Liu, Z.Y. Li, X.J. Yuan, B.L. Wu. *J. Coord. Chem.*, **65**, 3721 (2012).